crystals

MDPI

Supplementary Materials

Unexpected Selective Gas Adsorption on A 'Non-Porous' Metal Organic Framework

Stuart Beveridge [1,2], Craig A. McAnally [1,2], Gary S. Nichol [3], Alan R. Kennedy [2], Edmund J. Cussen [2] and Ashleigh J. Fletcher [1,*]

Crystallographic Data

Measurements were made with an Oxford Diffraction Xcalibur E instrument. The structure was refined to convergence against F^2 using all unique reflections. Refinement used SHELXL-2014 as implemented within WINGX [1, 2]. The anions and the solvent molecules have relatively large displacement parameters as is common for small units within the cavities of a MOF. In the final model only one BF_4 unit was modelled as disordered. Appropriate restraints and constraints were applied to this disordered anion to ensure that all fragments had approximately normal bond distances and displacement behaviour. Selected crystallographic and refinement data are given in Table SI1 and atomic coordinates are in Table SI2. Full structural data is available in cif format as CCDC 2008488.

1. G. M. Sheldrick. Acta Cryst. 2015, C71, 3-8.

2. L. J. Farrugia. J. Appl. Cryst. 2012, 45, 849-854.

Table 1. Crystal Data and Structure Refinement for $[Cu(tpt)][BF_4]\cdot\frac{3}{4}H_2O$.

Empirical formula	**$C_{18}\ H_{13.50}\ B\ Cu\ F_4\ N_6\ O_{0.75}$**
Formula weight	476.20
Temperature	123(2) K
Wavelength	0.71073 Å
Crystal system	Monoclinic
Space group	Cc
Unit cell dimensions	a = 19.6546(8) Å
	b = 17.9133(6) Å
	c = 24.0581(11) Å
	B = 112.816(5) °
Volume	7807.6(6) $Å^3$
Z	16
Density (calculated)	1.620 Mg/m^3
Absorption coefficient	1.178 mm^{-1}
F(000)	3832
Crystal size	0.22 x 0.18 x 0.10 mm^3
Theta range for data collection	3.82 to 27.00°.
Index ranges	-25<=h<=25, -22<=k<=21, -30<=l<=30
Reflections collected	26295
Independent reflections	14509 [R(int) = 0.0284]
Completeness to theta = 27.00°	99.2 %
Absorption correction	Semi-empirical from equivalents
Max. and min. transmission	1.00000 and 0.93598
Refinement method	Full-matrix least-squares on F^2
Data / restraints / parameters	14509 / 99 / 1154
Goodness-of-fit on F^2	1.043
Final R indices [I>2sigma(I)]	R1 = 0.0510, wR2 = 0.1226
R indices (all data)	R1 = 0.0666, wR2 = 0.1341
Absolute structure parameter	0.009(6)

Largest diff. peak and hole	0.813 and -0.502 e.Å^{-3}

crystals

MDPI

Table SI2: Atomic coordinates ($x10^4$) and equivalent isotropic displacement parameters ($Å^2 x10^3$) for $Cu(tpt)BF_4 \cdot ¾H_2O$. U(eq) is defined as one third of the trace of the orthogonalized U^{ij} tensor.

Atom	x	y	z	U(eq)
Cu(1)	2434(1)	-8776(1)	-7379(1)	25(1)
Cu(2)	-1625(1)	-8864(1)	-4682(1)	32(1)
Cu(3)	4879(1)	-6173(1)	-2022(1)	26(1)
Cu(4)	4598(1)	-11238(1)	-2902(1)	24(1)
F(1)	3468(3)	-5954(3)	-5293(2)	80(2)
F(2)	4195(2)	-5046(2)	-4709(2)	50(1)
F(3)	3995(2)	-6111(2)	-4280(2)	55(1)
F(4)	4708(3)	-6137(3)	-4827(2)	95(2)
F(6)	-500(3)	-8795(2)	-2458(2)	61(1)
F(5)	92(3)	-8947(3)	-1471(2)	72(1)
F(9)	6484(4)	-9406(4)	-1590(4)	168(4)
F(10)	6250(4)	-9137(4)	-764(2)	130(3)
F(7)	-1027(3)	-8432(2)	-1833(2)	63(1)
F(11)	6536(4)	-8247(3)	-1253(3)	97(2)
F(12)	5453(3)	-8885(4)	-1685(3)	119(2)
F(13)	3453(12)	-11140(10)	-5180(5)	95(3)
F(14)	3686(10)	-10778(8)	-5988(8)	116(3)
F(15)	2599(7)	-11133(9)	-6123(7)	91(3)
F(16)	3521(11)	-12012(7)	-5905(11)	78(3)
F(8)	-894(2)	-9667(2)	-1970(2)	61(1)
O(1)	2574(3)	-7008(3)	-4892(3)	69(2)
O(2)	-3767(4)	-5990(4)	-4620(3)	92(2)
O(3)	7445(4)	-8744(4)	-2154(3)	83(2)
N(1)	3437(2)	-11011(2)	-9292(2)	22(1)
N(2)	4317(2)	-11449(2)	-8364(2)	19(1)
N(3)	4309(2)	-11931(2)	-9284(2)	21(1)
N(4)	2830(2)	-9517(2)	-7787(2)	23(1)
N(5)	6513(2)	-13196(2)	-7778(2)	23(1)
N(6)	2929(3)	-11346(2)	-11489(2)	28(1)
N(7)	-3607(2)	-8156(2)	-7756(2)	22(1)
N(8)	-2757(2)	-9071(2)	-7784(2)	20(1)
N(9)	-3644(2)	-8606(2)	-8694(2)	19(1)
N(10)	-2103(3)	-8776(3)	-5575(2)	34(1)
N(11)	-2122(3)	-10498(2)	-9280(2)	30(1)
N(12)	-5737(3)	-6754(2)	-9266(2)	25(1)
N(13)	1939(2)	-8693(2)	-3000(2)	19(1)
N(14)	1920(2)	-8251(2)	-3938(2)	20(1)
N(15)	1056(2)	-9161(2)	-3920(2)	21(1)
N(16)	4020(2)	-6817(2)	-2451(2)	25(1)
N(17)	355(3)	-8775(2)	-6135(2)	26(1)
N(18)	366(2)	-10515(2)	-2407(2)	24(1)
N(19)	1489(2)	-13570(2)	-3885(2)	21(1)
N(20)	1441(2)	-13065(2)	-4815(2)	26(1)
N(21)	587(2)	-13996(2)	-4810(2)	25(1)
N(22)	3687(2)	-11846(2)	-3308(2)	24(1)
N(23)	39(2)	-13647(3)	-7009(2)	27(1)
N(24)	6(2)	-15497(2)	-3299(2)	22(1)
C(1)	3740(3)	-11027(3)	-8699(2)	19(1)
C(2)	4573(3)	-11892(3)	-8684(2)	21(1)
C(3)	3738(3)	-11479(3)	-9568(2)	21(1)
C(4)	3435(3)	-10511(3)	-8364(2)	19(1)
C(5)	2850(3)	-10041(3)	-8695(2)	22(1)
C(6)	2570(3)	-9560(3)	-8393(3)	27(1)
C(7)	3386(3)	-9989(3)	-7472(3)	24(1)
C(8)	3701(3)	-10484(3)	-7745(2)	22(1)
C(9)	5236(3)	-12370(3)	-8355(2)	20(1)
C(10)	5620(3)	-12309(3)	-7730(2)	24(1)
C(11)	6262(3)	-12730(3)	-7459(2)	24(1)
C(12)	6119(3)	-13247(3)	-8375(2)	32(1)
C(13)	5491(3)	-12845(3)	-8678(2)	24(1)
C(14)	3455(3)	-11448(3)	-10230(2)	23(1)
C(15)	3597(3)	-12017(3)	-10571(3)	32(1)
C(16)	3311(4)	-11952(3)	-11196(3)	38(1)

C(17)	2811(4)	-10810(4)	-11155(3)	43(2)
C(18)	3055(4)	-10850(4)	-10538(3)	43(2)
C(19)	-3036(3)	-8622(3)	-7484(3)	26(1)
C(20)	-3061(3)	-9038(3)	-8381(3)	21(1)
C(21)	-3884(3)	-8175(3)	-8357(2)	20(1)
C(22)	-2703(3)	-8665(3)	-6817(3)	25(1)
C(23)	-2885(4)	-8160(4)	-6470(3)	42(2)
C(24)	-2559(4)	-8217(4)	-5854(3)	42(2)
C(25)	-1942(4)	-9263(4)	-5913(3)	47(2)
C(26)	-2234(4)	-9221(4)	-6538(3)	42(2)
C(27)	-2747(3)	-9546(3)	-8702(2)	20(1)
C(28)	-2186(3)	-10023(3)	-8381(3)	29(1)
C(29)	-1901(3)	-10485(3)	-8681(3)	34(1)
C(30)	-2661(3)	-10026(3)	-9596(3)	30(1)
C(31)	-2989(3)	-9551(3)	-9328(3)	27(1)
C(32)	-4530(3)	-7689(3)	-8678(2)	20(1)
C(33)	-4893(3)	-7709(3)	-9295(2)	25(1)
C(34)	-5495(3)	-7255(3)	-9571(3)	28(1)
C(35)	-5371(3)	-6731(3)	-8665(3)	26(1)
C(36)	-4776(3)	-7191(3)	-8354(3)	25(1)
C(37)	2186(3)	-8264(3)	-3342(2)	19(1)
C(38)	1343(3)	-8713(3)	-4213(2)	19(1)
C(39)	1373(3)	-9123(3)	-3316(2)	20(1)
C(40)	2825(3)	-7769(3)	-3022(2)	19(1)
C(41)	3184(3)	-7771(3)	-2401(2)	24(1)
C(42)	3789(3)	-7287(3)	-2122(3)	25(1)
C(43)	3664(3)	-6820(3)	-3048(2)	23(1)
C(44)	3067(3)	-7275(3)	-3361(2)	24(1)
C(45)	1016(3)	-8743(3)	-4875(3)	22(1)
C(46)	1275(3)	-8290(3)	-5219(2)	36(1)
C(47)	934(4)	-8322(4)	-5838(3)	42(2)
C(48)	124(4)	-9217(3)	-5790(3)	36(1)
C(49)	420(3)	-9207(4)	-5168(3)	38(2)
C(50)	1045(3)	-9602(3)	-2982(2)	22(1)
C(51)	435(4)	-10047(3)	-3315(3)	37(2)
C(52)	119(3)	-10482(3)	-3013(3)	35(1)
C(53)	950(3)	-10073(3)	-2093(3)	29(1)
C(54)	1297(3)	-9611(3)	-2370(2)	25(1)
C(55)	1731(3)	-13113(3)	-4210(2)	23(1)
C(56)	881(3)	-13519(3)	-5091(2)	24(1)
C(57)	913(3)	-13989(3)	-4208(3)	21(1)
C(58)	2401(3)	-12665(3)	-3883(3)	23(1)
C(59)	2769(3)	-12707(3)	-3274(2)	24(1)
C(60)	3413(3)	-12282(3)	-2995(2)	24(1)
C(61)	3312(3)	-11812(3)	-3905(2)	30(1)
C(62)	2689(3)	-12204(3)	-4211(2)	27(1)
C(63)	576(3)	-13548(3)	-5755(2)	25(1)
C(64)	493(3)	-12914(3)	-6103(2)	30(1)
C(65)	219(3)	-12975(3)	-6725(2)	32(1)
C(66)	125(3)	-14254(3)	-6666(2)	30(1)
C(67)	369(4)	-14241(3)	-6054(3)	34(1)
C(68)	603(3)	-14502(3)	-3887(3)	20(1)
C(69)	15(3)	-14963(3)	-4207(3)	25(1)
C(70)	-268(3)	-15440(3)	-3904(3)	25(1)
C(71)	585(3)	-15051(3)	-2984(3)	23(1)
C(72)	890(3)	-14551(3)	-3260(2)	21(1)
B(1)	4085(5)	-5820(5)	-4783(4)	54(2)
B(2)	-581(5)	-8965(4)	-1928(3)	43(2)
B(3)	6168(7)	-8901(6)	-1315(5)	70(3)
B(4)	3324(6)	-11321(5)	-5763(4)	91(3)
F(18)	1929(10)	-11596(8)	-5592(7)	78(3)
F(17)	3023(10)	-10912(12)	-5112(8)	95(3)
F(19)	1763(13)	-10434(12)	-5442(10)	116(3)
B(5)	2285(10)	-10909(10)	-5510(9)	91(3)
F(20)	2395(12)	-10717(10)	-6027(9)	91(3)
F(14A)	3864(8)	-10867(8)	-5373(7)	116(3)
F(13A)	3026(8)	-11650(8)	-5361(6)	95(3)

F(15A)	2834(8)	-10996(8)	-6274(6)	91(3)
F(16A)	3707(11)	-11897(7)	-5900(11)	78(3)

Purification of 2,4,6-tri(4-pyridyl)-1,3,5-triazine (tpt)

The synthesis of TPT was successfully carried out and produced a quantity of 4.4 g (14 mmol) of dark brown crystallised product straight from the autoclave. This was removed by washing out with water and vacuum filtering to remove water from the product, and represent a yield of 48.7% with respect to 4-cyanopyridine.

By washing through with a 50/50 EtOH/H_2O mixture over a vacuum filtration set up, large quantities of impurities were removed and upon drying, a lighter brown solid was present. The clear solvent solution turned a light brown indicating impurities had been dissolved, and upon further vacuum filtration, a light brown product was collected. After drying, the final product was weighed and a final mass of 3.4 g (10.8 mmol) was recorded, giving a final yield of 37.7% with respect to 4-cyanopyridine

IR spectroscopy, pre- and post-purification (Figure SI1) shows several peaks expected for tpt, with pyridine ring vibrations at 1520 cm^{-1} and 1575 cm^{-1}; triazine ring vibrations at 1370 cm^{-1} and 1320 cm^{-1}; and weak C=N bending at 1065 cm^{-1} and 1050 cm^{-1}, all of which correlate to literature values.[1] Purification results in peak refinement, whilst maintaining correlation with literature values.

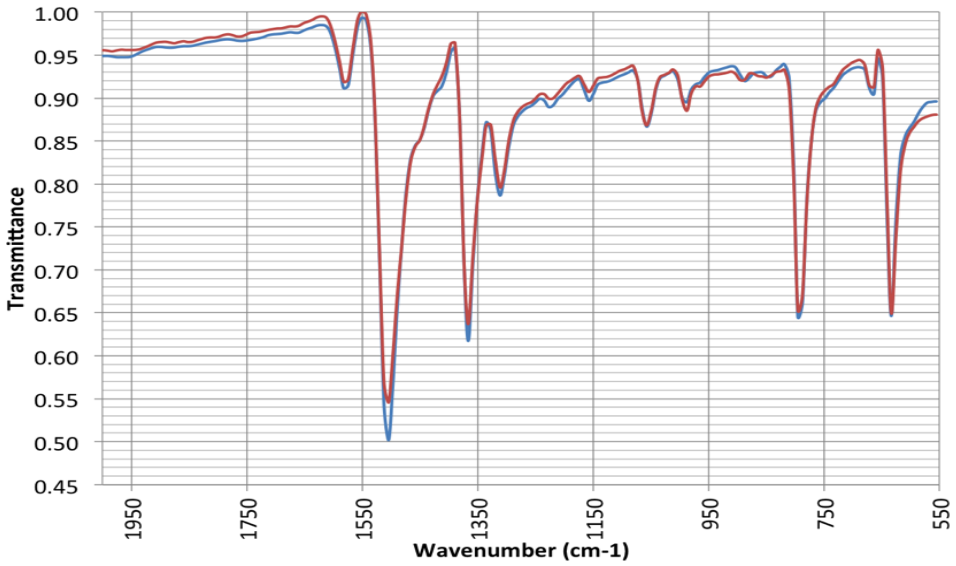

Figure SI1: IR Spectra of unpurified tpt (blue), and purified tpt (red).

Characterization data

Consistency of Synthesis

Phase purity was confirmed using powder X-ray diffraction; all key peaks were present at the same reflection angles within all samples (Figure SI2), and comparison of single and powder X-ray diffraction data showed excellent agreement (Figure SI3).

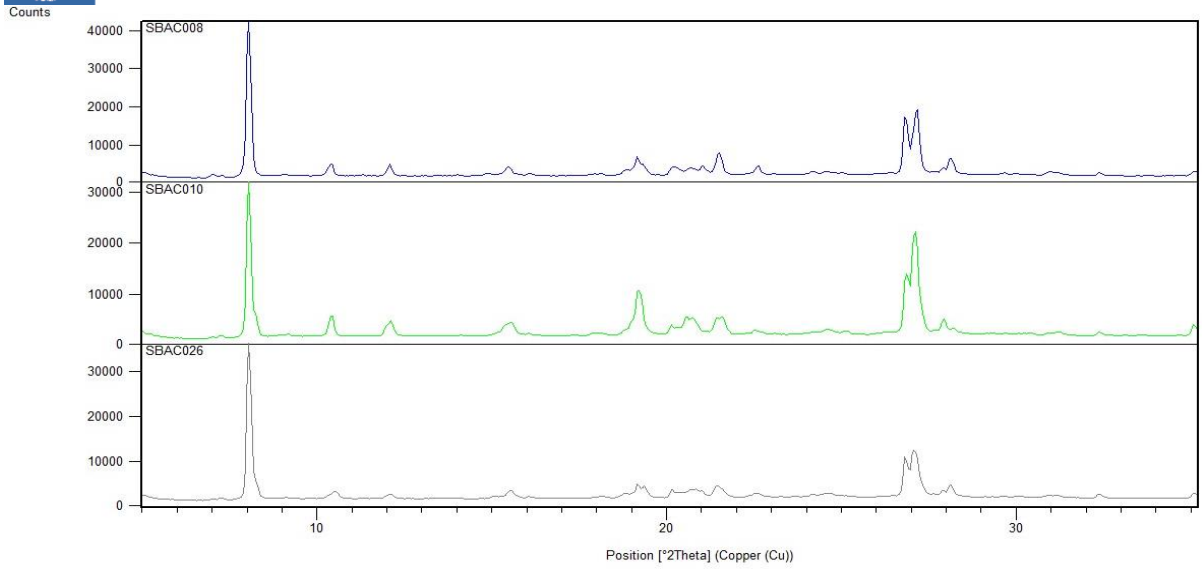

Figure SI2: Comparison of PXRD across three produced samples of the produced MOF.

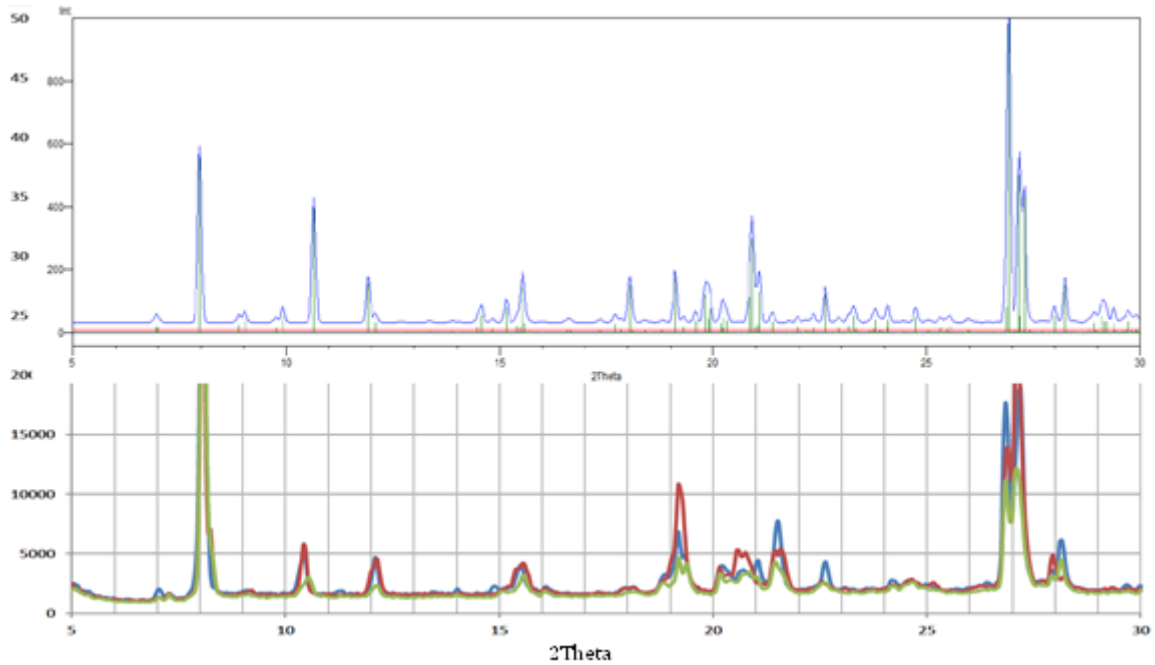

Figure SI3: Comparison of: (top) Simulated powder X-ray diffraction pattern based upon single crystal analysis; (bottom) Experimental powder X-ray diffraction patterns for three different samples.

Thermal stability and heat capacity of $Cu(tpt)BF_4 \cdot ¾H_2O$

The thermal stability of $Cu(tpt)BF_4 \cdot ¾H_2O$ was determined using thermal gravimetric analysis (TGA) *[Perkin Elmer TGA7] and* differential scanning calorimetry (DSC) *[Mettler Toledo HPDSC827].* The data (Figure SI4) indicate a very thermally strong material, with only ~4.5% of mass lost during analysis; a consequence of π-stacked interpenetrating layers. Water molecules account for 2.8% of the materials formula by weight, and the difference is attributed to methanol loss from the porous network as a result of incomplete solvent exchange.

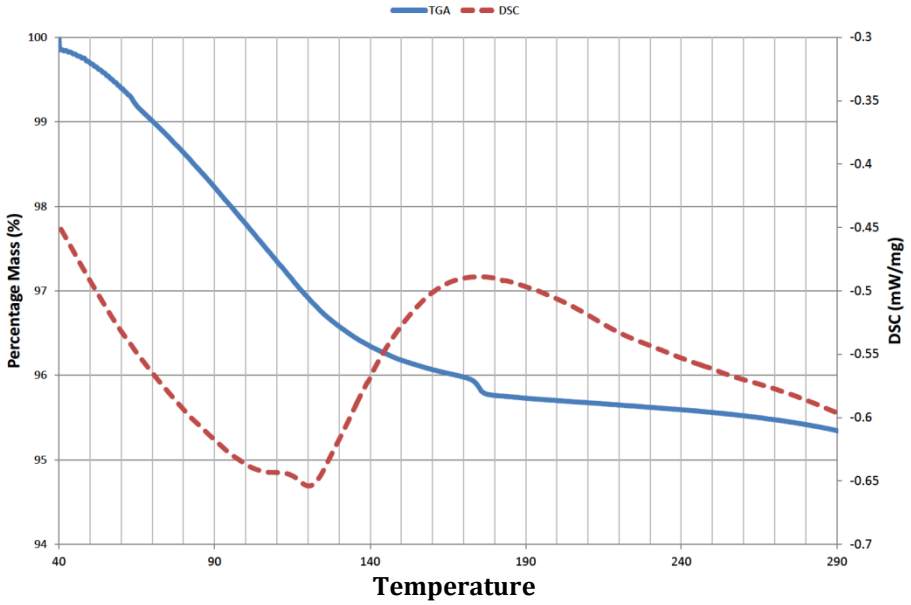

Figure SI4: TGA and DSC of Cu(tpt)BF_4·¾H_2O.

The heat capacity (Cp) was determined using TGA and DSC data; the Cp value was significantly distorted by loss of guest species (40˚C - 170˚C), due to the increase in thermal energy adsorbed (Figure SI5). Hence, the region of 180˚C – 290˚C was chosen as a linear approximation; Equation 1 was utilized to determine Cp.

$$C_p = \left(\frac{1}{m}\right)\frac{\Delta Q}{\Delta T} \qquad \text{Equation 1}$$

Where: ΔQ is rate of change in heat flow; ΔT is rate of change of temperature; and m is sample mass.

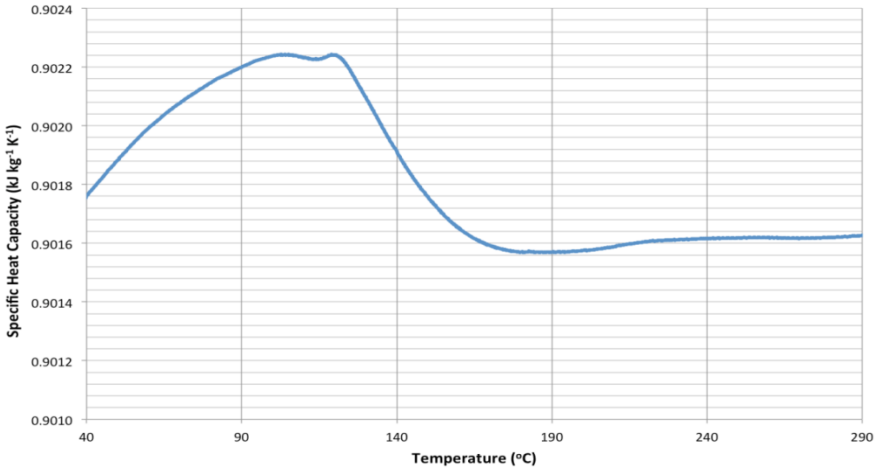

Figure SI5: Calculated heat capacity across the full DSC range of 40˚C-290˚C.

TGA data was used to accurately determine the true sample mass at each respective temperature; assuming that all guest species had been lost, and the resulting thermal energy input was all absorbed by the material during heating, extrapolation gave a Cp value of 0.902 kJ kg^{-1} K^{-1} (0.429 kJ mol^{-1} K^{-1}), at 298K.

Determination of surface area

Volumetric adsorption of N_2 on Cu(tpt)BF_4·¾H_2O at 77 K gave the poorly defined isotherm shown in Figure SI6.

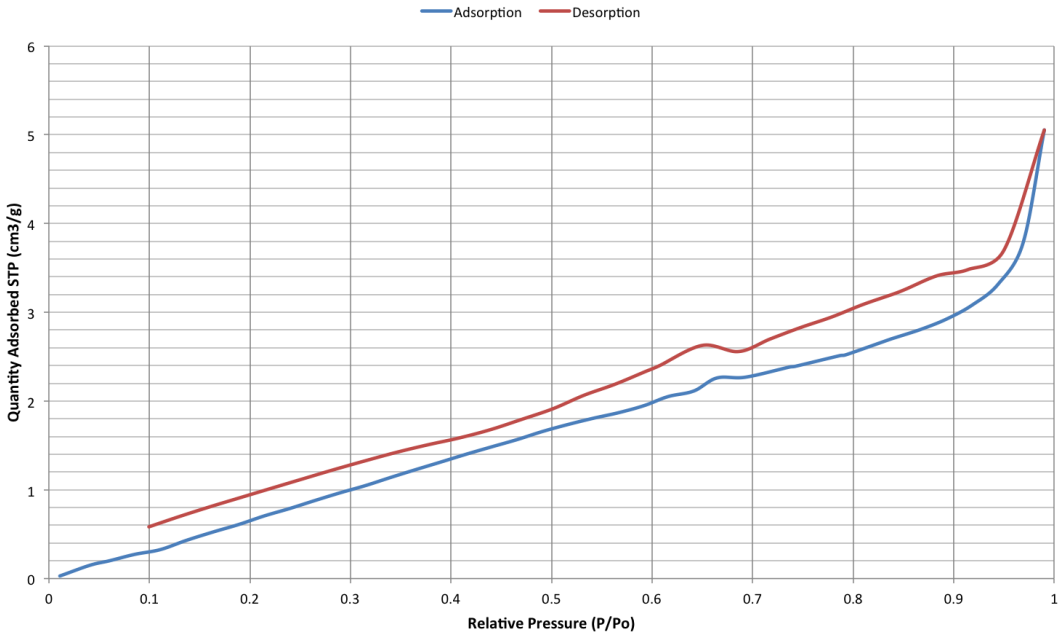

Figure SI6: Adsorption isotherm for N_2 on Cu(tpt)BF_4·¾H_2O at 77 K.

Langmuir analysis[2] was inappropriate for the data obtained (evaluation gave a negative monolayer volume), hence, BET analysis[3] was used. The overall quantity of N_2 adsorbed is low compared to similar materials; this is due to the small micropores within the material restricting nitrogen adsorption, resulting in activated diffusion.

The adsorption data was analyzed using the Rouquerol transform of the BET method, which requires that a number of conditions are met to validate the calculated surface area.[4] These criteria are:

1. A linear fit is required from the selected relative pressure range, with an R^2 value close to unity.
2. The BET 'C' term must be a positive value, as a negative value would be meaningless due to its exponential derivative.
3. The Rouquerol transform $n(1-P/P_o)$ should increase with P/P_o for the selected BET relative pressure range, as proposed by Keii *et al.*[5]

4. The monolayer capacity (n_m) should be within the range selected as BET relative pressure parameters. This confirms that the value of n_m falls within the applied BET range, and is not found though extrapolation.
5. The value of $1/(\sqrt{C}+1) \approx P/P_o$ at monolayer capacity, n_m. This provides a consistency check and can also be used to further optimize the selection of the BET relative pressure range if this condition is not met.

The modified plot for N_2 adsorption on Cu(tpt)BF_4·¾H_2O (Figure SI7) shows a decrease at P/Po = 0.11, which distorts the linear best fit line required. It is standard practice to select points around such data,[6] therefore the section of P/Po = 0.04 – 0.11 was selected for further analysis.

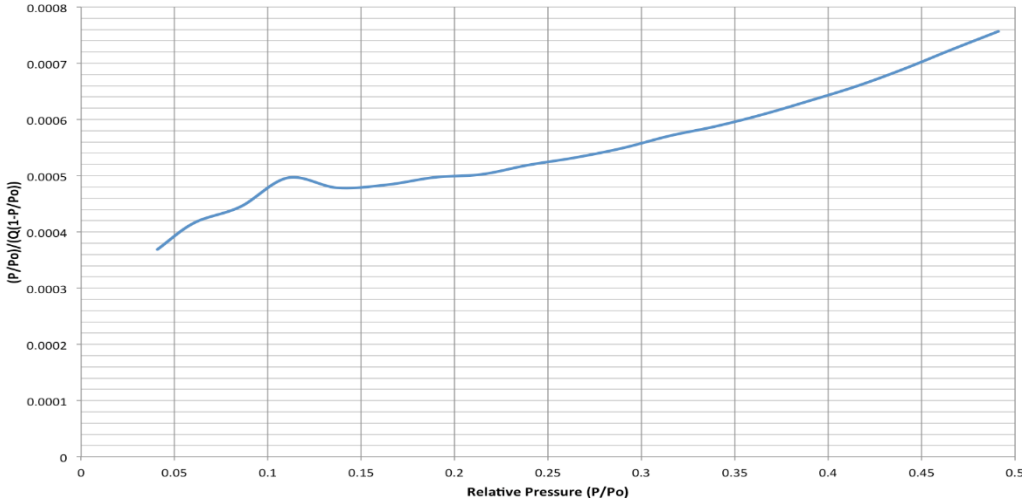

Figure SI7: BET plot from Rouquerol transform data for adsorption of N_2 on Cu(tpt)BF_4·¾H_2O at 77 K.

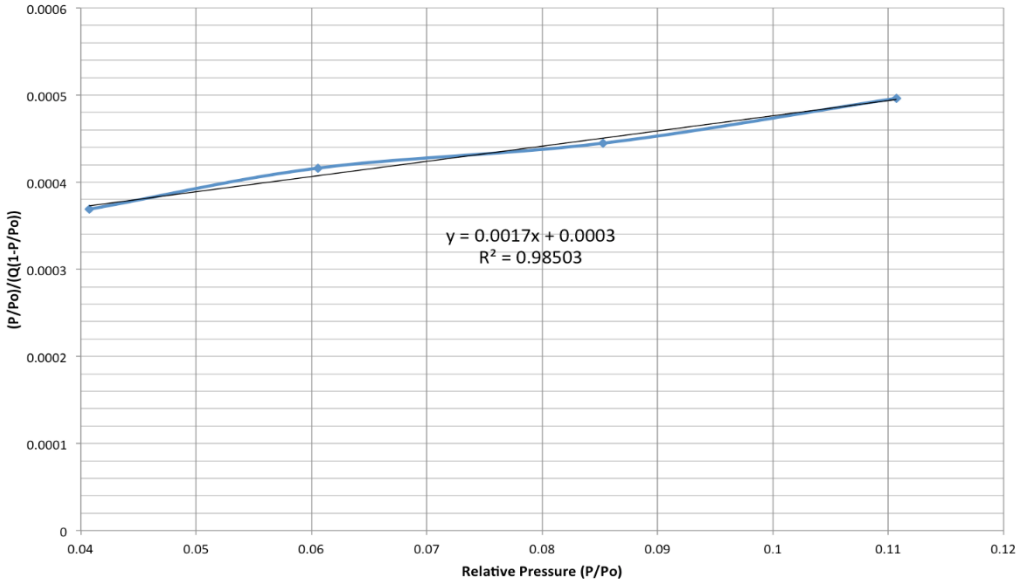

Figure SI8: Selected area (0.04≤P/P_o≤0.11) BET fit for adsorption of N_2 on Cu(tpt)BF_4·¾H_2O at 77 K.

The corresponding surface area is 2177 m^2/g, compared to 6.5 $m^2\ g^{-1}$ determined by traditional BET analysis, but the narrow data range (Figure SI8) and unfeasible value of v_m (500 $cm^3\ g^{-1}$) limit the validity of this analysis.

It is recognized that the quadrupole moment of CO_2 can affect the surface area determined, however, analysis was performed to provide an effective CO_2 adsorption surface area, and to confirm activated diffusion with respect to N_2 adsorption.

Langmuir analysis of the CO_2 adsorption isotherm for Cu(tpt)BF_4·¾H_2O at 273 K is shown in Figure SI9.model, the CO_2 adsorption isotherm correlates almost perfectly to the model.

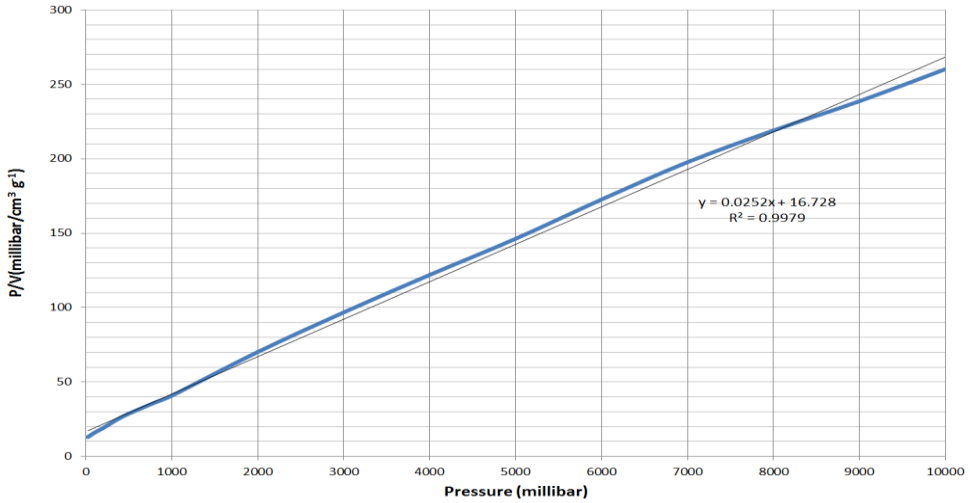

Figure SI9: Adsorption isotherm for CO_2 on Cu(tpt)BF_4·¾H_2O at 273K modeled to Langmuir adsorption model.

The resulting surface area is 208 m^2 g^{-1} for a sample outgassed at 353 K (200 m^2 g^{-1} for outgassing at 433 K).

References

1. Furutani, Y.; Kandori, H.; Kawano, M.; Nakabayashi, K.; Yoshizawa, M.; Fujita, M. In situ spectroscopic, electrochemical, and theoretical studies of the photoinduced host− guest electron transfer that precedes unusual host-mediated alkane photooxidation. *Journal of the American Chemical Society* **2009,** *131* (13), 4764-4768.
2. Langmuir, I. The constitution and fundamental properties of solids and liquids. Part i. Solids. *Journal of the American Chemical Society* **1916,** *38*, 2221.
3. Brunauer, S.; Emmett, P. H.; Teller, E. Adsorption of gases in multimolecular layers. *Journal of the American Chemical Society* **1938,** *60*, 309-319.
4. Llewellyn, P. L.; Rodriquez-Reinoso, F.; Rouqerol, J.; Seaton, N.; Rouquerol, J.; Llewellyn, P.; Rouquerol, F. Is the BET equation applicable to microporous adsorbents? *Studies in Surface Science and Catalysis* **2007,** *160*, 49-56.
5. Keii, T.; Takagi, T.; Kanetaka, S. A new plotting of the BET method. *Analytical Chemistry* **1961,** *33* (13), 1965-1965.
6. Moellmer, J.; Celer, E.; Luebke, R.; Cairns, A. J.; Staudt, R.; Eddaoudi, M.; Thommes, M. Insights on adsorption characterization of metal-organic frameworks: a benchmark study on the novel soc-MOF. *Microporous and Mesoporous Materials* **2010,** *129* (3), 345-353.